

Domain orbital state in ferromagnetic insulating $\text{La}_{0.825}\text{Ca}_{0.175}\text{Mn}_{0.99}\text{Fe}_{0.01}\text{O}_3$ compound

M. Pissas, G. Papavassiliou, E. Devlin and A. Simopoulos

Institute of Materials Science, NCSR, Demokritos, 15310 Aghia Paraskevi, Athens, Greece

V. Likodimos

Department of Applied Mathematics and Physics,

National Technical University of Athens, 157 80 Athens, Greece

(Dated: November 18, 2018)

Using Mössbauer and EPR spectroscopy we have studied the insulating ferromagnetic $\text{La}_{1-x}\text{Ca}_x\text{Mn}_{0.99}\text{Fe}_{0.01}\text{O}_3$ ($x = 0.175$) compound prepared in air and reduced atmosphere. The average hyperfine field follows a mean field approximation solution in contrast with the ferromagnetic metallic regime where it significantly deviates from the order parameter deduced from neutron diffraction data or mean field approximation. Although the magnetic measurements show remarkable differences between air prepared and reduced R samples the corresponding Mössbauer spectra are almost identical. The strong temperature dependance of the hyperfine field distribution at the ^{57}Fe nucleus is related with the supertransferred magnetic field between ferric ion and the oxygen bridged six nearest-neighbor manganese ions. The sudden increasing of the width of the hyperfine field distribution above $T_B \approx 100$ K has been attributed to the orbital disordering occurring for $T > T_B$.

PACS numbers: 87.64Pj,75.47.Lx,75.50.Dd,87.64.Hd

Apart from the large number of works dedicated in the study of $\text{La}_{1-x}\text{Ca}_x\text{MnO}_3$ compound the detailed elucidation of its ground state is yet an unresolved problem. The two end-compounds $x = 0$ and $x = 1$ are A and G-type antiferromagnets respectively. As Ca substitutes for La in LaMnO_3 compound, for $0 \leq x \leq 0.125$ the samples display an insulated canted antiferromagnetic (CA) ground state, changing to ferromagnetic insulated (FI) for $0.125 \leq x \leq 0.2$ and ferromagnetic metallic (FM) for $0.23 \leq x < 0.5$. The FI phase is one of the most unexpected phases in the physics of manganites since it has not been predicted neither by the double exchange model nor by any other. Furthermore, a number of experimental facts show that the ground state especially in the FI regime is not so simple. In the FI regime the magnetic measurements reveal, a paramagnetic to ferromagnetic transition and upon further cooling an additional anomaly is detected at $T_B \sim 100$ K. Neutron diffraction measurements¹ have provided evidences that the particular anomaly is related with an instability or a metastability with both magnetic and structural character. In the case of $\text{La}_{1-x}\text{Sr}_x\text{MnO}_3$ this transition has been attributed to an orbital ordered transition leading to a FI state.² ^{57}Fe Mössbauer spectroscopy is an extremely valuable tool in solid state physics. The long half-life of the 14.4 keV state yields a resonance linewidth narrow enough to permit resolution of nuclear fine and hyperfine structure in a spectrum. Microscopic probes, such as NMR and EPR are often of limited use, since their signals are being observable only under certain conditions, whereas in the case of ^{57}Fe Mössbauer spectroscopy one is virtually guaranteed of being able to observe a spectrum.

In manganese perovskites Mössbauer spectroscopy in low ^{57}Fe and ^{119}Sn -doped samples^{3,4,5,6,7,8,9,10,11} has con-

tributed useful information. As an example the sublattice magnetization can be determined directly from the hyperfine field. Using Mössbauer spectroscopy and electron spin resonance we investigate the FI regime of the phase diagram with emphasis to the microscopic origin of the intricate behavior below T_B using a sample with $x = 0.175$ which is in the middle of the ferromagnetic insulating regime.

I. EXPERIMENTAL DETAILS

A sample with nominal composition $\text{La}_{1-x}\text{Ca}_x\text{Mn}_{0.99}\text{Fe}_{0.01}\text{O}_3$ ($x = 0.175$) was prepared by the standard solid state reaction method using Fe_2O_3 90% enriched with ^{57}Fe . We prepared two samples. The first sample was prepared in air atmosphere in all stages of the preparation. We call this sample air prepared sample (AP). The second sample was annealed in the final stage of the preparation at 1000° in reduced atmosphere and we call this sample reduced sample (R). The x-ray diffraction data were analyzed using the Rietveld refinement method (assuming the orthorhombic $Pnma$ space group for both samples) and revealed single phase materials. Figure 1 shows part of the powder x-ray diffraction patterns for AP and R samples. The lattice parameters for the AS and R samples were determined to be $a = 5.4883(1)$ Å, $b = 7.7585(2)$ Å, $c = 5.5062(1)$ Å and $a = 5.5012(4)$ Å, $b = 7.7706(4)$ Å and $c = 5.5093(4)$ Å, for AP and R samples, respectively.

The absorption Mössbauer spectra (MS) were recorded using a conventional constant acceleration spectrometer with a $^{57}\text{Co}(\text{Rh})$ source moving at room temperature, while the absorber was kept fixed in a variable tempera-

ture cryostat equipped with a 6.5T superconductive magnet with the field being perpendicular to the γ -rays. The resolution was determined to be $\Gamma/2 = 0.12$ mm/sec using a thin α -Fe foil. DC magnetization measurements were performed in a SQUID magnetometer (Quantum Design).

ESR experiments were carried out on a Bruker ER 200D spectrometer at the X-band (9.41 GHz) with 100 kHz field modulation. The magnetic field was scaled with a NMR gaussmeter, while temperature dependent measurements were carried out in the range of 4-300 K employing an Oxford flow cryostat upon heating from the lowest temperature. Measurements were performed using either fine powdered samples dispersed in high vacuum grease or small ceramic pieces (mass of 1-2 mg), a small portion of which was exposed to the maximum rf field in order to avoid over-loading the resonant cavity.²⁰

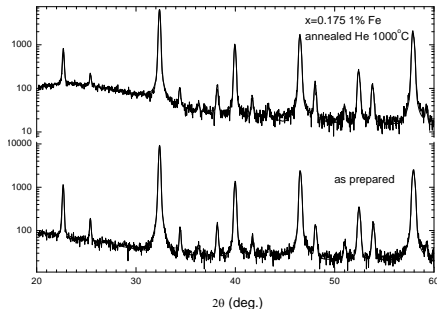


FIG. 1: X-ray diffraction patterns of (AP) and (R) samples in semilogarithmic plot.

II. MAGNETIC MOMENT MEASUREMENTS

Figure 2(a) shows the temperature dependence of the dc-magnetic moment (m) in a field of 100 Oe for the AP and R samples respectively measured using the SQUID magnetometer. For both samples the data were collected on heating (zero field cooling branch ZFC) and on cooling (field cooling branch FC). Initially the sample was cooled at 4.2 K under zero magnetic field. Both measurements show a sharp ferromagnetic transition at 180 K and 190 K for the (R) and (AP) sample respectively. In addition, strong irreversibility between ZFC and FC branch has been observed for both samples at a temperature (T_{irr}), slightly below T_c . Furthermore, the ZFC branch displays a step like increase with onset temperature $T_B \sim 80$ K and 90 K for the AP and R samples respectively. Figure 2(b) shows the corresponding with Figure 2(a) ac-susceptibility measurements. For both samples the temperature where the irreversibility starts, in dc measurements, χ' is reduced, while the sharp drop which observed in dc measurements is displayed only by the AP sample. The R sample shows only a shoulder and only in the χ'' an anomaly is revealed. The reduction of χ' for $T < T_{irr}$

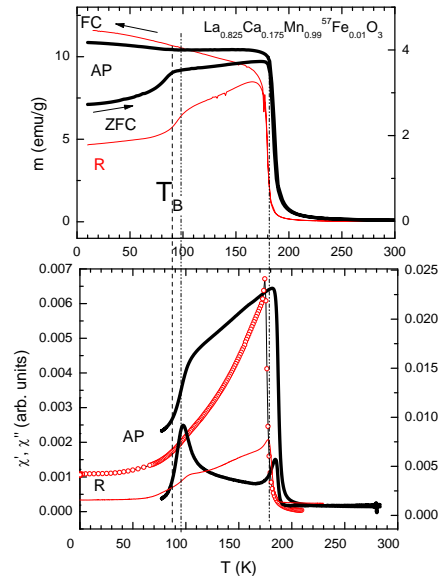


FIG. 2: (a) Temperature dependence of the magnetic moment at $H = 100$ Oe and (b) ac susceptibility of AP (thick line) and R (thin line) samples.

sometimes is an indication for spin glass behavior. However, this behavior can also be attributed to the domain wall dynamics. Simply the T_{irr} represents the temperature where pinning of the domain wall gives rise to a finite coercivity. Nevertheless, it is difficult to attribute the sharp drop at T_B to the increasing of the coercivity. One may argue that the step like increase of the $m_{ZFC}(T)$ at T_B corresponds to first order transition. However, the FC branch shows a slope change of the m_{FC} at T_B , indicative for a second order transition. Although we are not dealing with equilibrium states -as the hysteretic behavior implies- the overall behavior at T_B is unusual. It is not clear to the authors why the change of the magnetization in the FC and ZFC branches is in opposite directions. All the experimental data advocate for a glassy transition. It is interesting to compare the present magnetic measurements with those of the $\text{La}_{1-x}\text{Sr}_x\text{MnO}_3$ at FI regime occurring at $x = 0.125$. This compound exhibits a cooperative Jahn-Teller first-order transition at $T_{JT} \approx 270$ K, first a transition towards a ferromagnetic and metallic state, at $T_c = 181$ K and then, a magneto-structural first-order transition into a ferromagnetic and insulating state, at $T_B = 159$ K. This FI transition is characterized by a jump in the magnetization^{2,12,13,14}, typical for first-order transition, delta function-like variation of the specific heat, appearance of superstructure peaks, significant decreasing of the orthorhombicity and the three characteristic Mn-O distances become very close to each other. In addition Moussa et al.¹⁵ have found a splitting of the spin waves, an opening of a gap at $\mathbf{q} = (0, 0, 1/2)$ ($Pnmb$ notation) and a locking of the spin wave energy

on the energy values of phonons. In a $\text{La}_{1-x}\text{Ca}_x\text{MnO}_3$ $x = 0.175$ sample prepared in reduced atmosphere we also observed reduction of the orthorhombicity of the O' phase for $T < T_B$.¹⁶ This transition was not observed in the AP sample. All these features occurring at T_B , are indicative for a phase transition, most probably related with a new orbital/charge order.²

III. MÖSSBAUER SPECTRA

Figures 3 and 4 show the temperature variation of the Mössbauer spectra of the AP and R samples, respectively. At $T = 300$ K the spectra for both samples consist of a line which can be fitted by an unresolved doublet, keeping constant the line width to the value found from the calibration. The isomer shift $\delta = 0.37$ mm/s is characteristic for high spin iron Fe^{+3} in octahedral environment. The small value of the quadrupole's Hamiltonian eigenvalue $\epsilon = 0.08$ mm/s indicates that for the particular x the crystal structure at $T = 300$ K does not display cooperative Jahn-Teller distortion. This value agrees with the crystallographic data, according to the so-called O* structure ($c > a > b/\sqrt{2}$) which is present at $T = 300$ K. In this structure the octahedra are nearly undistorted and rotated with respect to the ideal perovskite structure. It is interesting to note that similar values for ϵ were found for $x = 0.25$ and 0.33 compounds.^{3,8} As temperature passes the Curie temperature the spectra become magnetically split. Near T_c the spectra are rather complicated consisting of a distribution of hyperfine fields and a paramagnetic component. By further cooling, the paramagnetic component gradually disappeared, whereas the width of the hyperfine field distribution decreased. At $T = 4.2$ K, for both R and AP samples, only one sextet is present with hyperfine parameters ($H_{hf} = 526(1)$ kOe, $\delta = 0.506(2)$ mm/s, $\epsilon = 0.038(2)$ mm/s), and ($H_{hf} = 530(1)$ kOe, $\delta = 0.506(2)$ mm/s, $\epsilon = 0.023(1)$ mm/s), respectively. These hyperfine parameters are common for Fe^{+3} in an octahedral coordination and in the high spin state $S = 5/2$.

The spectra in the intermediate temperatures were fitted by using the Le Caer-Dubois program¹⁷. In this method the relative transmission $I(i)$ in channel i ($i = 1, \dots, N$) is the convolution of a continuous hyperfine field distribution, with a sextuplet of Lorentzian peaks in the thin absorber approximation theoretically defined by $I(i) = I_0 - \int_0^\infty p(H)L(i, H)dH$, where I_0 is the background far from resonance. $L(i, H)$ defines the contribution in channel i of the elementary sextuplet. After discretization of the convolution integral $I(i) = I_0 - \sum_{k=1}^K \alpha_k \Delta H p(H_k)L(i, H_k)$ the unknowns $p_k \equiv p(H_k)$ can be determined by the least-squares minimization of $S = \sum_{i=1}^N W_i (I_e(i) - I(i))^2 + \lambda \int_0^\infty (d^2 p(H)/dH^2)^2 dH$, subject to $p_k \geq 0$. Here $I_e(i)$ is the experimental number of counts in channel i , W_i the corresponding weight, and λ is the smoothing parameter. In our case a value 50 has been used for the smoothing parameter. The resulting

hyperfine field distributions $p(H)$ for both samples are depicted in the insets of Fig. 5. At $T = 4.2$ K $p(H)$ is centered at about 525 kOe with a $\text{FWHM} \equiv \Delta H \approx 15$ kOe. This broadening is present up to 60 K. For $T > 60$ K the FWHM of the $p(H)$ increases linearly with temperature, up to T_c . Interestingly, in order to account for the region of the spectrum near $\nu = 0$ it is necessary $p(H)$ to be extended down to $H = 0$. This part of $p(H)$ is more pronounced as T_c is approached. Clearly, the temperature variation of the ΔH resembled the ZFC branch of the dc-magnetic moment or the real part of χ . If we accept a scenario that for $T < T_B$ an orbital ordering occurs, inside the FI phase, the orbital freedom for $T > T_B$ is responsible for the temperature dependence of ΔH . At this point we must note that the temperature variation of ΔH is different with that observed in $x = 0.33, 0.5$ and 0.6 samples.^{8,9,10} In these cases $p(H)$ shows a tail in the low field part. As temperature increases this tail spreads out to lower fields. In $x = 0.175$ case the main peak broadens but in a "symmetric fashion". The presence of the component with hyperfine field near zero may arise for several reasons. Presumably, this part of the distribution concerns atoms which experience a resultant exchange field via superexchange interactions with NN spins for which the energy $g\mu_B H$ is not large with respect to kT . Such atoms belong to regions where the iron ions destroy the ferromagnetic structure at a temperature different from this of the undoped sample. Another explanation can be given supposing that iron behaves as a magnetic impurity inside a ferromagnetic host, so that the part of $p(H)$ near $H = 0$ represents thermally populated states with $\langle H \rangle_T = 0$.

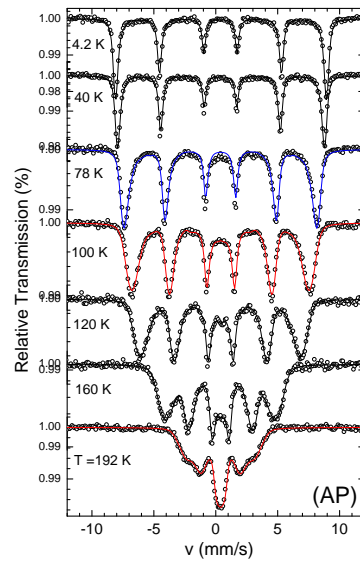


FIG. 3: Mössbauer spectra of (AP) sample.

We turn now to the microscopic origin of the hyperfine field distribution as it is revealed in MS. In ferric oxides contributions to H_{hf} from orbital angular momentum and conduction-electron polarization are rigorously

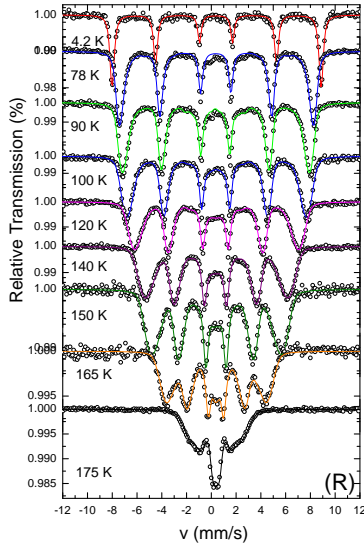


FIG. 4: Mössbauer spectra of (R) sample.

absent, while those from dipolar sources are small. This leaves only the contact field, proportional to the **net** polarization of s -electron density at the nucleus in question, as relevant for these systems. The contact field (H_{con}) is the vector sum of a local part \mathbf{H}_{loc} and a supertransferred part \mathbf{H}_{ST} . \mathbf{H}_{loc} is proportional to the local $3d$ spin \mathbf{S}_0 on the ion ($S = 5/2$ for the case of Fe^{+3}) while \mathbf{H}_{ST} is the resultant contributions from all single-ligand-bridged ferric nearest neighbors n , each proportional to the electronic spin \mathbf{S}_n on the NN cation site. The resulting field is:

$$\mathbf{H}_{hf} \approx H_{con} = -C(\mathbf{S}_0/S) + \sum_n B_n(\mathbf{S}_n/S) \quad (1)$$

where C and B_n are positive scalar parameters.¹⁸ The B_n parameters are associated with the geometry of coordination and can be expressed as a function of the Fe-O-Fe or Fe-O-Mn bond angle ϕ_n , namely $B_n = H_\pi + (H_\sigma - H_\pi) \cos^2 \phi_n$. In this equation the fields $H_{\pi,\sigma}$ arise from overlap distortions of the Fe cation s orbitals caused by the ligand p orbitals having been unpaired by spin transfer via π and σ bonds into unoccupied $3d$ orbitals on the NN cations n . In the case of insulating manganites although the mean value of H_{hf} is dominated by H_{loc} , the fluctuations ΔH_{hf} which generate the distribution of H_{hf} about its average are almost exclusively due to fluctuations in the supertransferred field. In our case $H_{loc} + H_{ST} = -530$ kOe (-the minus sign means that H_{hf} is antiparallel to the iron spin). By virtue of theoretical calculations¹⁸ it has been deduced that $H_{loc} \approx -450$ kOe in octahedral oxygen coordinated ferric iron, a fact implying that the iron moment must be antiferromagnetically coupled with the six nearest-neighbor manganese ions. Most importantly, if the Fe is ferromagnetically coupled with NN Mn ions, then this coupling will produce positive supertransferred field resulting in $H_{hf} < 450$ kOe,

contrary to the experimental findings. This antiferromagnetic coupling is experimentally verified by taking spectra in the presence of an external field (vide infra). Therefore, the abrupt increase of the width of the hyperfine field distribution is related to the change in fluctuations in the supertransferred field. We speculate that these fluctuations are related with the orbital domains or a new orbital state, formed at T_B . Above T_B the manganese e_g orbitals fluctuate due to the orbital disorder, producing significant fluctuations in the supertransferred field. Oppositely, below T_B orbitally-ordered domains are formed leading to freezing of the orbital disorder and subsequent reduction of the supertransferred magnetic field fluctuations. Our conclusions are further supported by Mössbauer results on the $\text{LaMn}_{0.99}\text{Fe}_{0.01}\text{O}_3$, which display the so-called A-antiferromagnetic structure with four ferromagnetic and two antiferromagnetic bonds. In this case $H_{hf}(0) \approx 450$ kOe,¹⁹ due to the positive contribution of the four (planar) ferromagnetic bonds and the negative one of the two (apical) antiferromagnetic bonds to the supertransferred field. It is noticeable that while the magnetic measurement of the AP sample is different from that of R sample, the resulting hyperfine distributions are practically similar. At this point we would like to discuss our Mössbauer results in comparison with the NMR ones. NMR spectra at 4.2 K for $\text{La}_{1-x}\text{Ca}_x\text{MnO}_3$ ($x \approx 0.175$) show a rich line shape. Basically, the line shape consists of two peaks corresponding to Mn^{+3} , Mn^{+4} and broad spectral features at intermediate frequencies attributed to mixed Mn valence states. Our results clearly show at $T = 4.2$ K only one sextet which corresponds to high spin ($S = 5/2$) Fe^{+3} state. In addition, the line width corresponds to small spread of the hyperfine field in the iron site. Basically iron sees though the exchange field $\mathbf{H}_{ex} = \sum_{n=1}^6 J_n \mathbf{S}_n$ a vector sum of the six NN manganese spins (J_n is the exchange constant). Broad distribution of the exchange fields, at $T = 4.2$ K, is expected only if there are several NN $\text{Mn}^{3+}, \text{Mn}^{4+}$ configurations. As the spectrum at $T = 4.2$ K shows, the fluctuations of the exchange field are near the resolution of the Mössbauer spectroscopy, a fact implying that the iron sees a unique NN configuration. Of course we have supposed that the iron has only manganese ions as NN, an approximation which is good so bad for 1% iron substituted for Mn ions. Figure 6 displays spectra taken in the presence of an external magnetic field of 60 kOe directed perpendicular to the propagation of γ -rays at selective temperatures. We notice that the spectrum at $T = 4.2$ K corresponds to a hyperfine field of 588 kOe, which is larger by 60 kOe than the spectrum taken at zero external field. Furthermore the intensity of the absorption peaks are in the ratio of 3:4:1 indicating that the Fe magnetic moments are in the direction of the external magnetic field. The increase of the hyperfine field by 60 kOe on the other hand shows that the moments (due to the negative sign of the H_{hf} are antiparallel to the external field. This can happen only if the Fe moments are antiferromagnetically coupled to

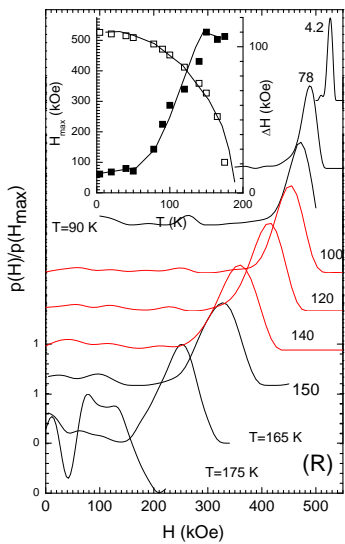
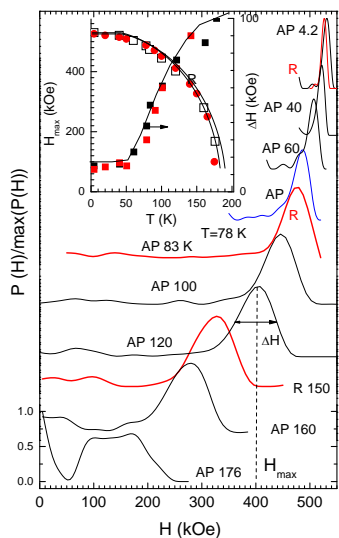


FIG. 5: Temperature dependence of the magnetic hyperfine field of for (AP) and (R) samples.

the manganese moments (which in turn are parallel to the external field). A similar situation was encountered in the $x=0.33$ system⁸ while for the $x = 0.5$ system⁹ the Fe moment was ferromagnetically coupled to the Mn magnetic moments. The hyperfine field at higher temperatures exceeds the field at zero external field by more than 60 kOe indicating that the magnetic order extends far beyond the curie temperature ($T_c \approx 180$ K).

IV. ESR RESULTS

Figure 7 shows representative ESR spectra of the AP sample as a function of temperature. A single exchange narrowed resonance line at $g = 2.0$ due to the strongly coupled $\text{Mn}^{3+}\text{-Mn}^{4+}$ system²⁰, is observed in the para-

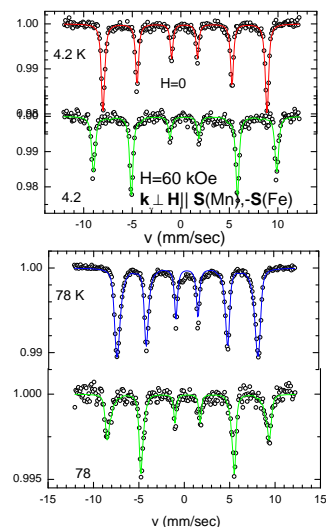


FIG. 6: Mössbauer spectra of R sample in the presence of an external magnetic field 60 kOe. The external magnetic field is perpendicular to the γ -rays. The zero magnetic field spectra are included in order to permit a direct comparison.

magnetic regime. The ESR line broadens and shifts to lower fields as the FM ordering transition is approached, while a single, broad ferromagnetic resonance (FMR) mode is observed below T_c , sustained down to the lowest investigated temperature for both powder and bulk specimens.

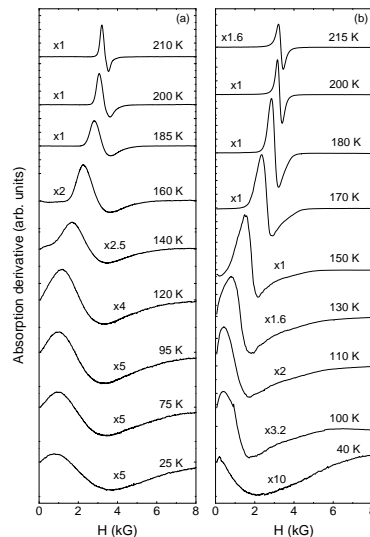


FIG. 7: Temperature dependence of the ESR spectra for (a) powder and (b) bulk samples of the (AP) sample at 9.41 GHz. The scale of each spectrum is multiplied by the indicated factors.

The resonance line is well fitted to a single Lorentzian lineshape in the whole temperature range, including both

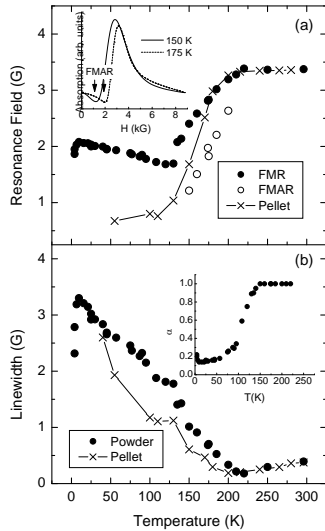


FIG. 8: Temperature dependence of the (a) resonance field and (b) linewidth for the (AP) samples. The inset in (a) shows the dip in the absorption curve of the powdered samples from which the antiresonance field (FMAR) is determined. The inset in (b) shows the temperature variation of the absorption-to-dispersion ratio (a).

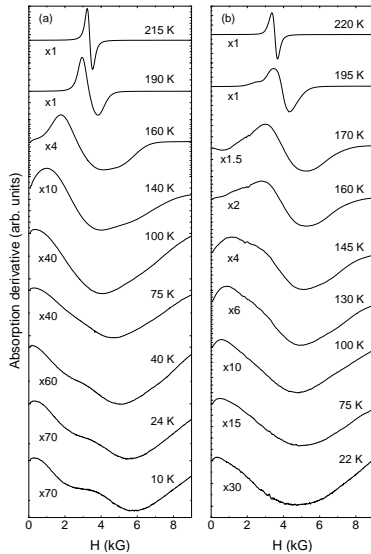


FIG. 9: Temperature dependence of the ESR spectra for (a) powder and (b) bulk samples of (R) samples at 9.41 GHz. The scale of each spectrum is multiplied by the indicated factors.

absorption and dispersion components to account for the skin effect pertaining even for powder samples, as well as the tail of the resonance absorption at negative field, a consequence of the linearly polarized rf field that becomes important when the width becomes comparable to the resonance field.²¹ Figure 8 summarizes the temperature dependence of the resonance field H_r and the linewidth ΔH (half-width at half-height). A small shift

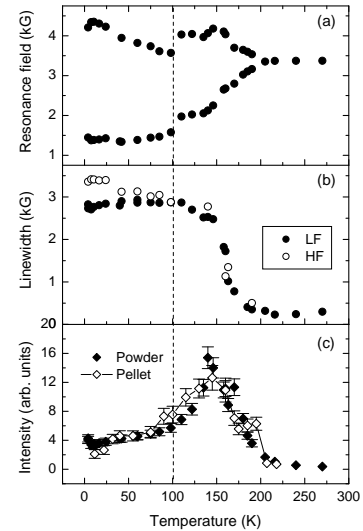


FIG. 10: Temperature dependence of the (a) resonance fields, (b) linewidths and (c) the total integrated intensity determined from the ESR spectra of the powdered (R) samples at 9.41 GHz.

of H_r is derived already from 250 K, in the paramagnetic phase, pertinent to the presence of demagnetizing fields and the built up of internal fields due to anisotropic interactions.²² At $T < T_c$, a substantial shift of the FMR mode is observed down to approximately 120 K, where a minimum of H_r is reached, most clearly evinced for the powder sample that is less affected by demagnetizing effects. This temperature variation complies qualitatively with the combined effects of magnetocrystalline anisotropy and demagnetizing fields, whose contribution is expected to be most pronounced for the powder and the bulk specimens, respectively [Fig. 8(a)]. Integration of the FMR lineshape yields a dip in the absorption spectra [inset of Fig. 8(a)], characteristic of the ferromagnetic antiresonance (FMAR) mode, which has been previously observed in other manganites.^{23,24,25,26} The variation of the corresponding resonance field is included in Fig. 8(a) in the temperature range of 150-200 K, where ΔH is sufficiently narrow for FMAR to be identified, yet not possible to be reliably analyzed for specimens whose shape is not well-defined²⁷. The linewidth goes through a minimum in the paramagnetic phase at $T_{\min} = 215 \text{ K} = 1.1T_c$ [Fig. 8(b)], reflecting the presence of static correlations well above T_c , rather than any critical behavior.^{28,29} Below T_c , a continuous increase of ΔH is observed that saturates for the powder specimen only at 15 K, suggestive of magnetic inhomogeneity.³⁰ Previous studies have shown that a spread of T_c , hardly observable by other methods, may account for the peak in the FMR linewidth near T_c ,³¹ while demagnetizing effects due to pores and surface irregularities in ceramic materials could be the main source of inhomogeneous broadening of ΔH at $T < T_{\min}$.³² Such a behavior that is proportional to

the average magnetization may accordingly account for the linewidth broadening down to $T = 100$ K, where the magnetization nearly saturates. However, these effects can not explain the small, though distinct increase of H_r and the excessive broadening of the FMR mode, most pronounced for the bulk sample at $T < 100$ K. A substantial increase of the resistivity can be also inferred at the same temperature from the absorption-to-dispersion ratio (α) plotted in the inset of Fig. 8(b), which decreases rapidly below 150 K and nearly saturates at 100 K, in agreement with the metal-insulator transition in this doping range.³³ Different spin dynamics may be thus invoked at $T < 100$ K to explain the FMR temperature evolution, most likely associated with a disordered FM phase complying with the marked anomalies of the dc and ac magnetic measurements. In that case, a different distribution of the anisotropy axes may also contribute to the FMR linewidth and the shift of H_r , especially for polycrystalline materials. It is worth noting that a single FMR line has been observed by high-frequency ESR for low-doped $\text{La}_{1-x}\text{Sr}_x\text{MnO}_3$ single crystals at $x = 0.15$ and 0.175 , which shifts or splits in two modes near structural transitions.²⁶ A single FMR mode has been also observed for epitaxial LCMO thin films with Mn-excess and higher Ca content ($x = 0.3$), showing an anomalous increase of ΔH at low temperatures³⁴. On the other hand, complicated FMR spectra have been reported for powdered LCMO single crystals with $x = 0.18$ in the temperature range of 100-400 K, suggesting the presence of phase separation, that complies favorably with the FMR data described below for the (R) samples.

Figure 9 shows typical ESR spectra obtained for the (R) samples at different temperatures. A single ESR line is observed only at $T > 200$ K in the paramagnetic regime, whereas a distorted lineshape comprising two broad FMR lines at low (LF) and high field (HF) with respect to $g = 2$, is evidenced at lower temperatures. This two-mode behavior, indicative of increased magnetic inhomogeneity, was verified for several bulk pieces, an example being shown in Fig. 9(b). In this case, a thin flake of the bulk ceramic (R) sample was measured with the magnetic field applied perpendicular to its plane, enhancing the HF line. The FMR spectra for the powder specimen that is less amenable to demagnetizing effects, could be well fitted using two Lorentzian lines without appreciable dispersion for $4\text{K} < T < 200$ K, except for the T -range of 150-180 K, where the lineshape was more distorted [Fig. 9(a)]. These results agree qualitatively with the FMR data reported for loose packed powders of LCMO single crystals with $x = 0.18$, where several FMR lines were resolved down to 150 K, where the conductivity also attains its maximum value.³³ Figure 10 shows the corresponding temperature variation of the resonant fields H_r , the linewidth ΔH and the doubly integrated intensity including in the latter case that of the bulk piece. The resonance field of the LF mode, which accounts for about 60-70% of the total intensity,

varies qualitatively similar to that of the (AP) sample, reaching an almost constant value below 100 K. Most importantly, an abrupt shift of both the LF and HF modes occurs at $T = 100$ K towards lower fields [Fig. 10(a)], accompanied by the broadening of the total FMR spectrum, mainly resulting from the HF line [Fig. 10(b)]. The total intensity reveals a maximum at $T = 145$ K for both specimens, though a shoulder appears in the vicinity of T_c for the bulk sample, followed by a relatively small decreasing trend below 100 K [Fig. 10(c)], which appears to resemble the ac susceptibility rather than the dc one, as previously noted.³³ A distorted FMR lineshape can be, in principle, expected for random powders with high magnetocrystalline and shape anisotropy.³⁴ However, comparison with the FMR and magnetization data of the (AP) samples clearly points to a dominant thermal treatment effect. The persistent anomalies of the FMR spectra for both samples at $T = 100$ K, indicate an intrinsically inhomogeneous magnetic ground state at low temperatures. This would further correlate with recent ¹³⁹La NMR revealing a freezing transition at $T_f = 80$ K³⁵, neutron scattering revealing a reentrant structural transition of the high-temperature pseudo-cubic phase at $T_B = 100$ K^{1,16}, as well as SR experiments showing a broad maximum of the spin-relaxation at $T = 110$ K for Ca doping in the $x = 0.17 - 0.18$ ³⁶.

V. CONCLUSIONS

Stoichiometric samples in the ferromagnetic insulating regime of $\text{La}_{1-x}\text{Ca}_x\text{MnO}_3$ compound $0.125 \leq x < 0.23$ display characteristic anomalies for $T < 100$ K, most probably related with an orbital transition. Our Mössbauer data revealed that the $\text{La}_{1-x}\text{Ca}_x\text{MnO}_3$ ($x = 0.175$) sample displays an anomaly in the temperature variation of the hyperfine field distribution of the probe ⁵⁷Fe nucleus which is related with supertransferred field. The change in the supertransferred field is closely connected with a new orbital transition at about $T = 100$ K. Our recent neutron diffraction results revealed¹⁶ that only the (R) samples display structural anomaly at $T = 100$ K. Furthermore, our Mössbauer spectra and magnetic measurements show this anomaly in both samples. We attribute this apparent discrepancy to the fact that this new orbital state in the (AP) samples is short ranged or glass type. Since the Mössbauer spectroscopy is a local probe it can detect changes that occur in local level. The conclusion from Mössbauer spectra is also in agreement with EPR data. In the EPR data inhomogeneities are present in both samples but are most pronounced in the (R) sample supporting further the interpretation for a new orbital state which is not long range order in (AP) samples. We believe that the present results close a gap in the literature concerning the physics of the (AP) and (R) samples in the ferromagnetic insulating regime.

-
- ¹ G. Biotteau, M. Hennion, F. Moussa, J. Rodríguez-Carvajal, L. Pinsard, A. Revcolevschi, Y. M. Mukovskii, and D. Shulyatev, *Phys. Rev. B* **64**, 104421 (2001).
- ² Y. Endoh, K. Hirota, S. Ishihara, S. Okamoto, Y. Murakami, A. Nishizawa, T. Fukuda, H. Kimura, H. Nojiri, K. Kaneko, and S. Maekawa, *Phys. Rev. Lett.* **82**, 4328 (1999).
- ³ M. Pissas, G. Kallias, E. Devlin, A. Simopoulos, and D. Niarchos, *J. Appl. Phys.* **81**, 8 (1997).
- ⁴ S. B. Ogale, R. Shreekala, Ravi Bathe, S. K. Date, S. I. Patil, B. Hannoyer, F. Petit, and G. Marest, *Phys. Rev. B*, **57**, 7841 (1998); B. Hannoyer, G. Marest, J. M. Greneche, Ravi Bathe, S. I. Patil, S. B. Ogale, *Phys. Rev. B* **61**, 9613 (2000).
- ⁵ A. Tkachuk, K. Rogacki, D. E. Brown, B. Dabrowski, A. J. Fedro, C. W. Kimball, B. Pyles, X. Xiong, Daniel Rosenmann, and B. D. Dunlap, *Phys. Rev. B* **57**, 8509 (1998).
- ⁶ A. Simopoulos, G. Kallias, E. Devlin, I. Panagiotopoulos, and M. Pissas, *J. Magn. Magn. Mat.* **177-181**, 860 (1998).
- ⁷ V. Chechersky, A. Nath, I. Isaac, J. P. Franck, K. Ghosh, H. Ju, and R. L. Greene, *Phys. Rev. B* **59**, 497 (1999); V. Chechersky, A. Nath, I. Isaac, J. P. Franck, K. Ghosh, and R. L. Greene, *J. Phys.: Condens. Matter* **11**, 8921 (1999).
- ⁸ A. Simopoulos, M. Pissas, G. Kallias, E. Devlin, N. Moutis, I. Panagiotopoulos, D. Niarchos, C. Christides, and R. Sonntag, *Phys. Rev. B* **59**, 1263 (1999).
- ⁹ G. Kallias, M. Pissas, E. Devlin, A. Simopoulos, and D. Niarchos, *Phys. Rev. B* **59**, 1273 (1999).
- ¹⁰ G. Kallias, M. Pissas, E. Devlin, A. Simopoulos, *Phys. Rev. B* **65**, 144426 (2001).
- ¹¹ A. Simopoulos, G. Kallias, E. Devlin, M. Pissas, *Phys. Rev. B* **63**, 054403 (2001).
- ¹² S. Uhlenbruck, R. Teipen, R. Klingeler, B. Bchner, O. Friedt, M. Hcker, H. Kierspel, T. Niemöller, L. Pinsard, A. Revcolevschi, and R. Gross, *Phys. Rev. Lett.* **82**, 185 (1999).
- ¹³ P. Wagner, I. Gordon, S. Mangin, V. V. Moshchalkov, Y. Bruynseraede, L. Pinsard, A. Revcolevschi, *Phys. Rev. B* **61**, 529 (2000).
- ¹⁴ G.-L. Liu, J.-S. Zhou, J. B. Goodenough, *Phys. Rev. B*, **64**, 144414, (2001).
- ¹⁵ F. Moussa, M. Hennion, F. Wang, P. Kober, J. Rodríguez-Carvajal, P. Reutler, L. Pinsard, and A. Revcolevschi, *Phys. Rev. B* **67**, 214430 (2003).
- ¹⁶ M. Pissas, unpublished results.
- ¹⁷ G. Le Caer and J. M. Dubois *J. Phys. E:Sci. Instrum.*, **12**, 1083 (1979).
- ¹⁸ G. A. Sawatzky and F. Van der Woude, *J. de Phys. (Paris) Colloq.* **12**, C6-47 (1974).
- ¹⁹ M. Pissas, A. Simopoulos, unpublished results.
- ²⁰ M. T. Causa, M. Tovar, A. Caneiro, F. Prado, G. Ibanez, C. A. Ramos, A. Butera, B. Alascio, X. Obradors, S. Pinol, F. Rivadulla, C. Vazquez-V Vazquez, M. A. Lopez-Quintela, J. Rivas, Y. Tokura, and S. B. Oseroff, *Phys. Rev. B* **58**, 3233 (1998).
- ²¹ V. A. Ivanshin, J. Deisenhofer, H.-A. Krug von Nidda, A. Loidl, A. A. Mukhin, A. M. Balbashov, and M. V. Eremin, *Phys. Rev. B* **61**, 6213 (2000).
- ²² N. O. Moreno, P. G. Pagliuso, C. Rettori, J. S. Gardner, J. L. Sarrao, J. D. Thompson, D. L. Huber, J. F. Mitchell, J. J. Martinez, and S. B. Oseroff, *Phys. Rev. B* **63**, 174413 (2001).
- ²³ S. T. Wang and C. W. Searle, *Can. J. Phys.* **49**, 387 (1971).
- ²⁴ J. S. Ramachandran, S. M. Bhagat, J. L. Peng, and M. Rubinstein, *Solid. State Commun.* **96**, 127 (1996).
- ²⁵ N. A. Viglin, S. V. Naumov, and Ya. M. Mukovskii, *Fiz. Tverd. Tela* **43**, 1855 (2001) [*Phys. Solid State* **43**, 1934 (2001)].
- ²⁶ D. Ivannikov, M. Biberacher, H.-A. Krug von Nidda, A. Pi-menov, A. Loidl, A. A. Mukhin, and A. M. Balbashov, *Phys. Rev. B* **65**, 214422 (2002).
- ²⁷ A. H. Morrish, *The Physical Principles of Magnetism* (Krieger Publishing, Florida, 1983).
- ²⁸ D. L. Huber, G. Alejandro, A. Caneiro, M. T. Causa, F. Prado, M. Tovar, and S. B. Oseroff, *Phys. Rev. B* **60**, 12 155 (1999).
- ²⁹ V. A. Atsarkin, V. V. Demidov, F. Simon, R. Gaal, Y. Mori-tomo, K. Conder, A. Janossy, and L. Forro, *JMMM* (2002).
- ³⁰ S. E. Lofland, S. M. Bhagat, H. L. Ju, G. C. Xiong, T. Venkatesan, and R. L. Greene, *Phys. Rev. B* **52**, 15 058 (1995).
- ³¹ M. Dominguez, S. E. Lofland, S. M. Bhagat, A. K. Raychaudhuri, H. L. Ju, T. Venkatesan, and R. L. Greene, *Solid State Commun.* **97**, 193 (1996).
- ³² F. Rivadulla, M. A. Lopez-Quintela, L. E. Hueso, J. Rivas, M. T. Causa, C. Ramos, R. D. Sanchez, and M. Tovar, *Phys. Rev. B* **60**, 11 922 (1999).
- ³³ V. Markovich, E. Rozenberg, A. I. Shames, G. Gorodetsky, I. Fita, K. Suzuki, R. Puzniak, D. A. Shulyatev, and Ya. M. Mukovskii, *Phys. Rev. B* **65**, 144402 (2002).
- ³⁴ F. P. Valstyn, J. P. Hanton, and A. H. Morrish, *Phys. Rev.* **128**, 2078 (1962).
- ³⁵ G. Papavassiliou, M. Belesi, M. Fardis, and C. Dimitropoulos, *Phys. Rev. Lett.* **87**, 177204 (2001).
- ³⁶ R. H. Heffner, J. E. Sonier, D. E. MacLaughlin, G. J. Nieuwenhuys, G. M. Luke, Y. J. Uemura, W. Ratcliff II, S.-W. Cheong, and G. Balakrishnan, *Phys. Rev. B* **63**, 094408